CHAPTER 4

ENHANCING THE THERMOELECTRIC PROPERTIES OF TiNiSn BY TRANSITION METALS CO-DOPED ON THE Ti-SITE OF $Ti_{0.5}TMI_{0.25}TMII_{0.25}NiSn$: A FIRST-PRINCIPLES STUDY

Introduction

Thermoelectric energy (TE) is an alternative energy source which directly converts heat to electrical energy. The performance of TE materials is specified by the dimensionless figure of merit; $ZT = (S^2\sigma/\kappa)T$, where S is the Seebeck coefficient, σ is electrical conductivity, κ is thermal conductivity and T is absolute temperature (Aswal, Basu & Singh, 2016). The TiNiSn half-Heusler alloy is a state-of-the-art *n*-type TE material with high TE performance at a mid-range temperature (Graf, Felser & Parkin, 2011). TiNiSn shows optimal S, σ, and κ, and yields an ZT equal to 0.4 at 600 – 800 K (Katayama, Kim, Kimura & Mishima, 2003). The Zr-substituted Ti-site of TiNiSn could have a reduced κ, while an Hf-substituted Ti-site could have an enhanced power factor ($S^2\sigma$) (Katayama et al., 2003). So far, Sakurada and Shutoh (2005) have had success in improving ZT from 0.4 to 1.2 and 1.5 at 700 – 800 K, for $Ti_{0.5}Zr_{0.25}Hf_{0.25}NiSn$ and $Ti_{0.5}Zr_{0.25}Hf_{0.25}NiSn_{0.998}Sb_{0.002}$, respectively. Although several research groups have explored and studied transition metal (TM)-doped Ti-sites, such as Nb (Muta, Kanemitsu, Kurosaki & Yamanaka, 2009), V (Lee, Tseng & Chao, 2010), Mn (Berry et al., 2017), or Sc (Stopa, Tobola, Kaprzyk, Hlil & Fruchart, 2006; Tobola, Jodin, Pecheur & Venturini, 2004), their ZT has always been less than that of Zr or Hf.

In addition, the TE properties of the TM–co–doped Ti–site of TiNiSn have not been reported. We proposed a theoretical study of the co–doping of the Ti–site of TiNiSn with transition metals such as Sc, Zr, Hf, V, Nb, or Mn, as $Ti_{0.5}TMI_{0.25}TMII_{0.25}NiSn$. The electronic structure, transport properties, and thermal conductivity were calculated with density functional theory, the Boltzmann transport equation, and molecular dynamics, respectively. The key point of this presentation is that the TM change the electronic structure, which affect to TE properties for *n*–type $Ti_{0.5}TMI_{0.25}TMII_{0.25}NiSn$.

Computational details

The TiNiSn and $Ti_{0.5}TMI_{0.25}TMII_{0.25}NiSn$ (where TMI and TMII are Sc, Zr, Hf, V, Nb, or Mn) atomic clusters were designed using an MgAgAs–type structure (Vilars & Calvert, 1991) with space group number 216. We used a conventional cell with the Wyckoff position: Ti1(0, 0, 0), Ti2(0, 0.5, 0.5), Ti3(0.5, 0, 0.5), Ti4(0.5, 0.5, 0), Ni1(0.75, 0.75, 0.75), Ni2(0.75, 0.25, 0.25), Ni3(0.25, 0.75, 0.25), Ni4(0.25, 0.25, 0.75), Sn1(0.5, 0, 0), Sn2(0.5, 0.5, 0.5), Sn3(0, 0, 0.5), and Sn4(0, 0.5, 0) for TiNiSn. In order to design $Ti_{0.5}TMI_{0.25}TMII_{0.25}NiSn$, we calculate total energy of TMI and TMII substitute in Ti–site. We found that the TMI substitute in Ti1(0, 0, 0) and TMII substitute in Ti2(0, 0.5, 0.5) are lowest energy. We employed the CIF2Cell package(Björkman, 2011) to make a TiNiSn and $Ti_{0.5}TMI_{0.25}TMII_{0.25}NiSn$ 2×2×2 supercell. The supercell composed of a total of 96 atoms showed $Ti_{32}Ni_{32}Sn_{32}$ for TiNiSn, and $Ti_{16}TMI_{8}TMII_{8}Ni_{32}Sn_{32}$ for $Ti_{0.5}TMI_{0.25}TMII_{0.25}NiSn$, as shown in Figure 23.

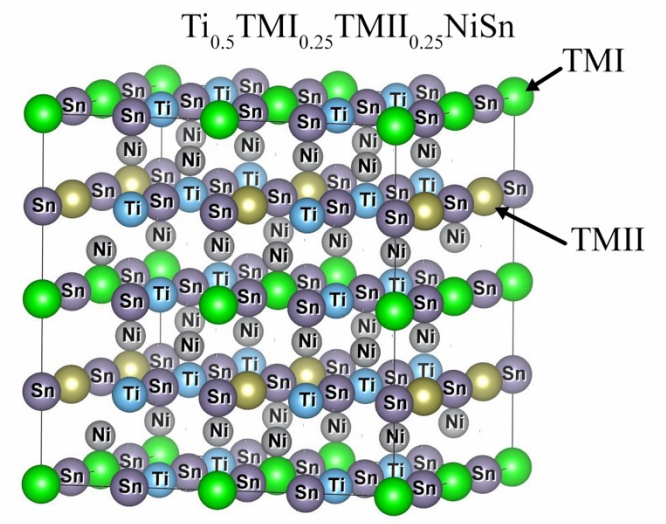

Figure 23 The $Ti_{0.5}TMI_{0.25}TMII_{0.25}NiSn$ crystal structure (TMI and TMII are Sc, Zr, Hf, V, Nb, or Mn).

The electronic structure was investigated by density functional theory (DFT) (Hohenberg & Kohn, 1964; Kohn & Sham, 1965) with a plane–wave self–consistent field implemented in the Quantum ESPRESSO package (P Giannozzi et al., 2017; Paolo Giannozzi et al., 2009). The Perdew–Burke–Ernzerhof (PBE) functional (Perdew, Burke & Ernzerhof, 1996) and generalized gradient approximations (GGA) (Rappe, Rabe, Kaxiras & Joannopoulos, 1990) were used for exchange–correlation. The 2×2×2 Monkhorst–Pack *k*–mesh Brillouin zone (BZ) integration, kinetic energy cut–off of 544 eV, and convergence threshold of 1×10^{-6} were used for self–consistent field calculation. This work was calculated with total charge equal to 0. The transport properties were investigated by Boltzmann transport theory with the constant scattering time approximation (CSTA) and Fourier interpolation of the calculated bands based on BoltzTraP code (Madsen & Singh, 2006). The transport properties were calculated with:

$$\sigma = \frac{1}{\Omega}\int \Xi(\varepsilon)\left[-\frac{\partial f_0}{\partial \varepsilon}\right] d\varepsilon, \tag{73}$$

$$S = \frac{1}{eT\Omega\sigma} \int \Xi(\varepsilon)(\varepsilon - \mu) \left[-\frac{\partial f_0}{\partial \varepsilon} \right] d\varepsilon, \quad (74)$$

$$\Xi(\varepsilon) = \sum \vec{v}_\alpha \vec{v}_\beta \, \tau, \quad (75)$$

where Ω is reciprocal space volume, f_0 is the Fermi–Dirac distribution function, ε is an eigen energy of each band structure, e is the electron charge, Ξ is the transport distribution, τ is the scattering time, $\vec{v}$ is the group velocity, and α and β are mean tensors. The total thermal conductivity (κ_{total}) for TiNiSn includes the electron (κ_{e}) and lattice (κ_{lat}) thermal conductivity. The value of κ_{e} was calculated by using the Wiedemann–Franz law as in the equations:

$$\kappa_{\mathrm{e}} = \sigma L T, \quad (76)$$

$$L = 1.5 + \exp[-\frac{|S|}{116}], \quad (77)$$

where L is the Lorenz number, and S is in μV K^{-1} (Kim, Gibbs, Tang, Wang & Snyder, 2015). Recently, molecular dynamics with the Green–Kubo relation (MD–GK) was used to successfully investigate the κ_{lat} of thermoelectric materials (Rittiruam et al., 2016). We employed Verlet's algorithm (Verlet, 1967) and Ewald's summation (Wigner, 1932), as implemented in MXDORTO code (Hirao & Kawamura, 1994), for MD simulation. The Morse–type (Morse, 1929) and Busing–Ida (Ida, 1976) functions were used for the potential function. The Nosé (Nosé, 1984) and Andersen (Andersen, 1980) methods were employed to control the temperature and pressure. The Green–Kubo relation for κ_{lat} can be expressed as:

$$\kappa_{\mathrm{lat}} = \frac{\Omega}{3k_B T^2} \int \langle \mathrm{J}(t)\mathrm{J}(0) \rangle \, dt, \quad (78)$$

where k_B is Boltzmann's constant, and J is an auto-correlation function. In order to improve the accuracy, κ_{lat} was calculated in 1×10^6 steps for the equilibrium state and an average taken over ten simulations with different auto-correlation functions. The MD was performed on an atomic cluster size 4×4×4 supercell with 768 atoms.

Results and Discussion

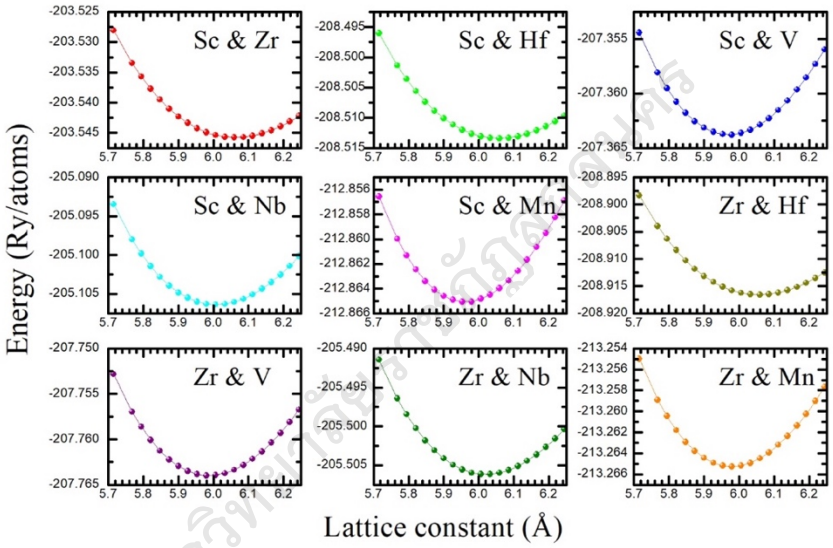

Figure 24 The calculated energy versus lattice constant for $Ti_{0.5}Sc_{0.25}Zr_{0.25}NiSn$ (Sc&Zr), $Ti_{0.5}Sc_{0.25}Hf_{0.25}NiSn$ (Sc&Hf), $Ti_{0.5}Sc_{0.25}V_{0.25}NiSn$ (Sc&V), $Ti_{0.5}Sc_{0.25}Nb_{0.25}NiSn$ (Sc&Nb) $Ti_{0.5}Sc_{0.25}Mn_{0.25}NiSn$ (Sc&Mn), $Ti_{0.5}Zr_{0.25}Hf_{0.25}NiSn$ (Zr&Hf), $Ti_{0.5}Zr_{0.25}V_{0.25}NiSn$ (Zr&V), $Ti_{0.5}Zr_{0.25}Nb_{0.25}NiSn$ (Zr&Nb), and $Ti_{0.5}Zr_{0.25}Mn_{0.25}NiSn$ (Zr&Mn).

First of all, we calculated the structure optimization with equilibrium structural parameters. The equilibrium structural parameters were obtained by evaluating the total energy variation with the lattice parameter as shown in Figures 24 and 25, and the results were fitted by the Murnaghan equation of state (Murnaghan, 1944). The equilibrium structural parameter is illustrated in Table 7. The calculated

lattice constant (a_0) value of 5.9534 Å for TiNiSn, previous literature of PBE–GGA approximation is ~5.9500 Å, (Kirievsky, Shlimovich, Fuks & Gelbstein, 2014; Wang et al., 2009) and the experimental is ~5.9400 Å (Hermet et al., 2014; Jung, Kurosaki, Kim, Muta & Yamanaka, 2010).

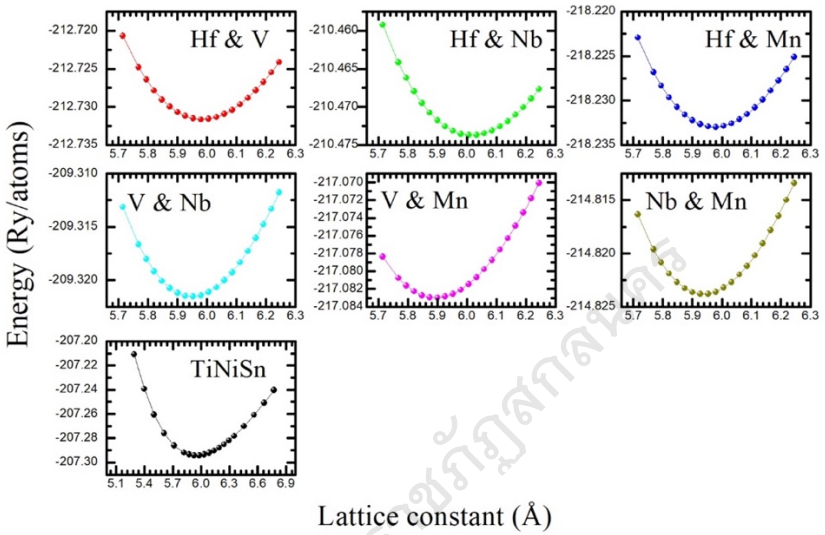

Figure 25 The calculated energy versus lattice constant for $Ti_{0.5}Hf_{0.25}V_{0.25}NiSn$ (Hf&V), $Ti_{0.5}Hf_{0.25}Nb_{0.25}NiSn$ (Hf&Nb), $Ti_{0.5}Hf_{0.25}Mn_{0.25}NiSn$ (Hf&Mn), $Ti_{0.5}V_{0.25}Nb_{0.25}NiSn$ (V&Nb) $Ti_{0.5}V_{0.25}Mn_{0.25}NiSn$ (V&Mn), $Ti_{0.5}Nb_{0.25}Mn_{0.25}NiSn$ (Nb&Mn), and TiNiSn

The calculated bulk modulus (B_0) is 124.39 GPa, which agrees with the experimental (Colinet, Jund & Tédenac, 2014) and theoretical (Kirievsky et al., 2014; Li et al., 2016) data for TiNiSn. The a_0 increased with substitution by ScZr, ScHf, ScV, ScNb, ScMn, ZrHf, ZrV, ZrNb, ZrMn, HfV, HfNb, and HfMn, but the VNb, VMn, and NbMn exhibit an a_0 less than that of TiNiSn. In TM co–substituted TI–site, the a_0 depends on the average atomic radius of Ti–site. For example, HfMn, considering the atomic radius written by the authors, have an average radius of 184.5 pm which is greater than the Ti one, 176 pm (Clementi, Raimondi & Reinhardt, 1967). In the same

way, the calculated E_0 of TiNiSn and $Ti_{0.5}TMI_{0.25}TMII_{0.25}NiSn$ have different values due to the E_0 of Ti, Sc, Zr, Hf, V, Nb and Mn also being different. The VNb, VMn, and NbMn show a higher B_0 than TiNiSn due to the B_0 being evaluated with $B_0 = -\mathrm{V}(\partial p/\partial \mathrm{V})_{\mathrm{V}=0}$, where p is the pressure which is calculated from $p = \partial E/\partial \mathrm{V}$.

Table 7 Equilibrium structural parameters: lattice constant (a_0), total energy (E_0), bulk modulus (B_0), and enthalpy of formation energy (E_f) for TiNiSn and $Ti_{0.5}TMI_{0.25}TMII_{0.25}NiSn$ (TMI and TMII are Sc, Zr, Hf, V, Nb, or Mn).

$Ti_{0.5}TMI_{0.25}TMII_{0.25}NiSn$	a_0 (Ang)	E_0 (Ry/atoms)	B_0 (GPa)	E_f (eV/formula)
TiNiSn	5.9534	−207.2942	124.59	−0.5641
$Ti_{0.5}Sc_{0.25}Zr_{0.25}NiSn$	6.0630	−203.5457	116.31	−0.5671
$Ti_{0.5}Sc_{0.25}Hf_{0.25}NiSn$	6.0587	−208.5134	118.42	−0.5358
$Ti_{0.5}Sc_{0.25}V_{0.25}NiSn$	5.9709	−207.3637	120.36	−0.5285
$Ti_{0.5}Sc_{0.25}Nb_{0.25}NiSn$	6.0077	−205.1063	123.59	−0.5558
$Ti_{0.5}Sc_{0.25}Mn_{0.25}NiSn$	5.9617	−212.8651	118.67	−0.4922
$Ti_{0.5}Zr_{0.25}Hf_{0.25}NiSn$	6.0568	−208.9165	122.96	−0.5619
$Ti_{0.5}Zr_{0.25}V_{0.25}NiSn$	5.9879	−207.7639	124.00	−0.5501
$Ti_{0.5}Zr_{0.25}Nb_{0.25}NiSn$	6.0208	−205.5616	128.14	−0.6607
$Ti_{0.5}Zr_{0.25}Mn_{0.25}NiSn$	5.9792	−213.2652	123.51	−0.5138
$Ti_{0.5}Hf_{0.25}V_{0.25}NiSn$	5.9842	−212.7316	126.14	−0.5188
$Ti_{0.5}Hf_{0.25}Nb_{0.25}NiSn$	6.0172	−210.4737	123.39	−0.5454
$Ti_{0.5}Hf_{0.25}Mn_{0.25}NiSn$	5.9754	−218.2329	124.76	−0.4826
$Ti_{0.5}V_{0.25}Nb_{0.25}NiSn$	5.9491	−209.3215	131.02	−0.5342
$Ti_{0.5}V_{0.25}Mn_{0.25}NiSn$	5.8932	−217.0829	128.90	−0.4748
$Ti_{0.5}Nb_{0.25}Mn_{0.25}NiSn$	5.9371	−214.8238	130.50	−0.4994

In order to study the stability of co-doping, we calculated the formation energy according to equations. (79) and (80):

$$E_f(\mathrm{TiNiSn}) = E(\mathrm{Ti_{32}Ni_{32}Sn_{32}}) - 32E^{\mathrm{bulk}}(\mathrm{Ti}) - 32E^{\mathrm{bulk}}(\mathrm{Ni}) - 32E^{\mathrm{bulk}}(\mathrm{Sn}), \quad (79)$$

$$E_f(\mathrm{Ti_{0.5}TMI_{0.25}TMII_{0.25}NiSn}) = E(\mathrm{Ti_{16}TMI_8TMII_8Ni_{32}Sn_{32}}) - 16E^{\mathrm{bulk}}(\mathrm{Ti}) - 8E^{\mathrm{bulk}}(\mathrm{TMI}) - 8E^{\mathrm{bulk}}(\mathrm{TMII}) - 32E^{\mathrm{bulk}}(\mathrm{Ni}) - 32E^{\mathrm{bulk}}(\mathrm{Sn}), \quad (80)$$

where $E(\mathrm{Ti_{32}Ni_{32}Sn_{32}})$ and $E(\mathrm{Ti_{16}TMI_8TMII_8Ni_{32}Sn_{32}})$ are the total energy of TiNiSn and $Ti_{0.5}TMI_{0.25}TMII_{0.25}NiSn$ obtained from the supercell. $E^{\mathrm{bulk}}(\mathrm{Ti})$, $E^{\mathrm{bulk}}(\mathrm{Ni})$,

$E^{\mathrm{bulk}}(\mathrm{Sn})$, $E^{\mathrm{bulk}}(\mathrm{TMI})$, and $E^{\mathrm{bulk}}(\mathrm{TMII})$ are the total energies in their bulk phases of Ti, Ni, Sn, and the transition metals, respectively. As Table I, the calculated E_f is −0.5641 eV/formula for un−doped. In TM co−doped, the E_f of ScZr, ScV, ZrHf, and ZrNb are less than un−doped, which means more stable than TiNiSn. So that, the ScHf, ScNb, ScMn, ZrV, ZrMn, HfV, HfNb, HfMn, VNb, VMn, and NbMn are stable less than TiNiSn. The calculated E_f shows that the structure of TiNiSn and the co−doped compounds are negative value, which is very stable. Therefore, a 50% co−doped TiNiSn exhibits a stable structure.

In order to discuss *n*−type TM−co−doped TiNiSn, we first considered the calculated total density of state and S. Our calculations show the total density of state (TDOS) with an energy gap (E_g) of 0.46 eV, which agrees with previous DFT work.(Douglas et al., 2014; Wang et al., 2009) The calculated TDOS of TiNiSn and $Ti_{0.5}TMI_{0.25}TMII_{0.25}NiSn$ are shown in Figure 26. The TDOS of ScV, ScNb, and ZrHf showed the valence band maximum (VBM) and minimum conduction band (MCB) at around −0.3 eV and 0.2 eV, respectively. The Fermi energies (E_F) of ScZr and ScHf are shifted down into the valence band, thus creating a hole−pocket (Zhang et al., 2016). ScMn, ZrV, ZrNb, ZrMn, HfV, HfNb, HfMn, VNb, VMn, and NbMn show the E_F shifting up into the conduction band, providing an electron−pocket. The calculated values of S depend on the chemical potential at 300 K, as shown in Figure 27.

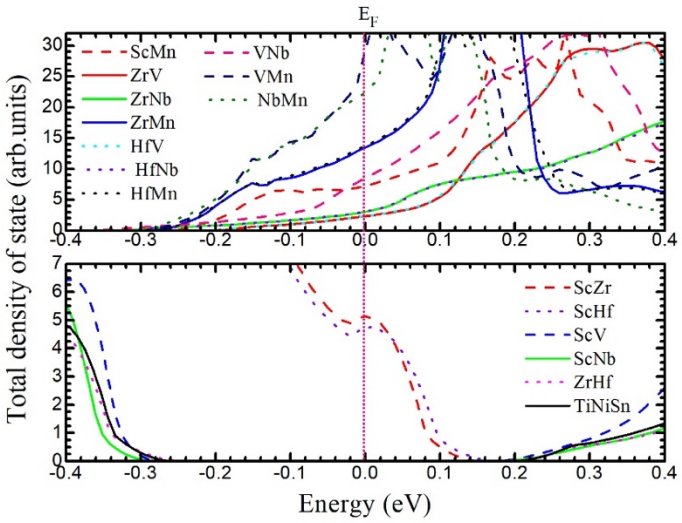

Figure 26 Total density of state (TDOS) of TiNiSn and $Ti_{0.5}TMI_{0.25}TMII_{0.25}NiSn$ (TMI and TMII are Sc, Zr, Hf, V, Nb, or Mn).

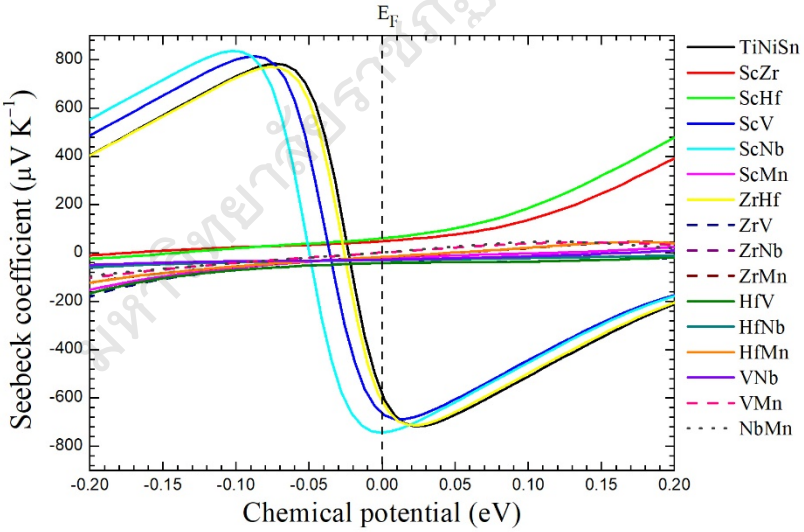

Figure 27 The Seebeck coefficients of TiNiSn and $Ti_{0.5}TMI_{0.25}TMII_{0.25}NiSn$ (TMI and TMII are Sc, Zr, Hf, V, Nb, or Mn) versus chemical potential at 300 K.

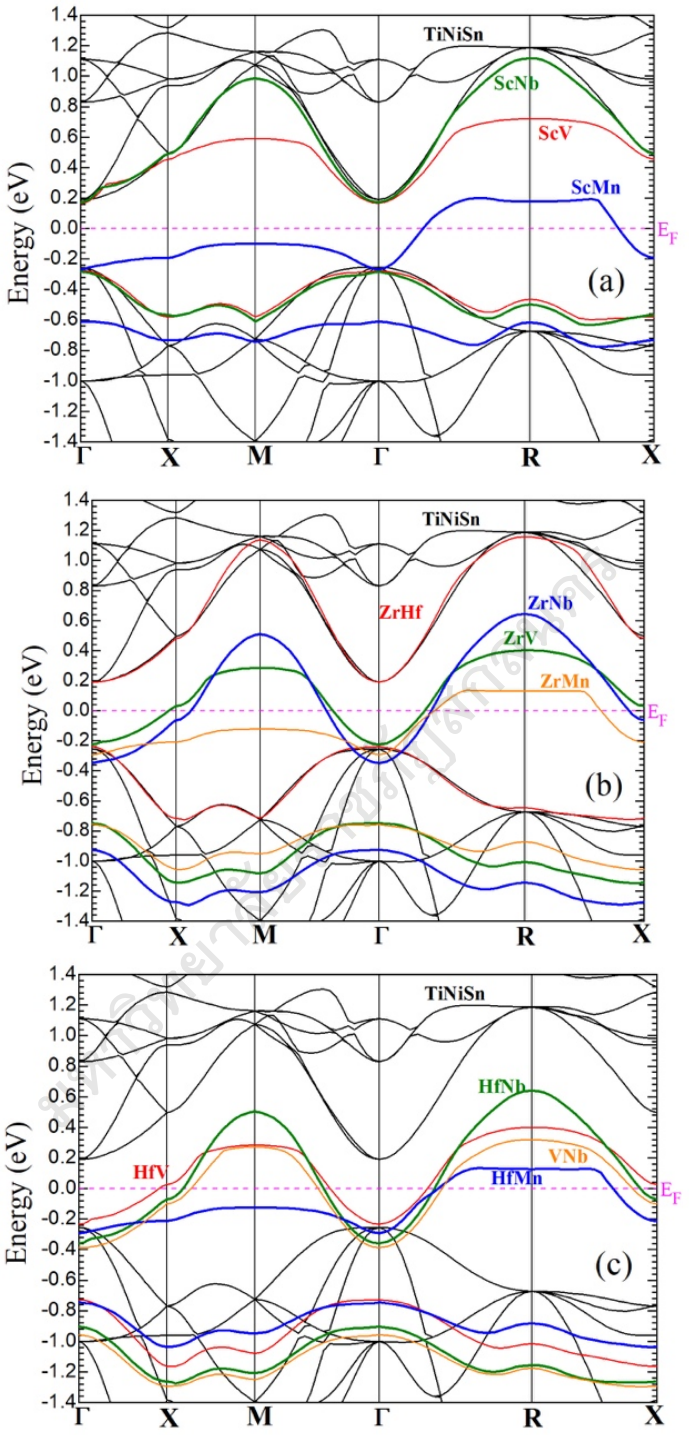

Figure 28 The band structure of TiNiSn (black line). The colored lines (green, red, and blue) represent the valence and conduction bands for $Ti_{0.5}TMI_{0.25}TMII_{0.25}NiSn$ composed ScV (a), ScNb (a), ScMn (a), ZrHf (b), ZrV (b), ZrNb (b), ZrMn (b), HfV (c), HfNb (c), HfMn (c), and VNb (c).

The E_F is exhibited at zero chemical potential. We considered the S around E_F and found that TiNiSn, ScV, ScNb, Sc*M*n, ZrHf, ZrV, ZrNb, Zr*M*n, HfV, HfNb, H*f*Mn, and VNb showed a negative value of S. The S values of ScZr, ScHf, V*M*n, and Nb*M*n exhibited a positive value. Generally, the negative and positive values of S mean *n*–type and *p*–type TE materials, respectively. The experimental (Bodak et al., 2004) and theoretical (Romaka et al., 2013) data showed that the Ti–site in TiNiSn substituted with Sc at 5 – 60% could be changed from *n*–type to *p*–type behavior. As is well known, the maximum ZT based on TiNiSn illustrated *n*–type behavior and never found in *p*–type (Sakurada & Shutoh, 2005). Therefore, we present results for *n*–type TE material.

The calculated band structure (BS) is illustrated in Figure 28. We present the VBM and CBM as colored lines for the TM–co–doped TiNiSn case. The BS of TiNiSn, ScV, ScNb, and ZrHf showed that the VBM and CBM occurred at the Γ point and provided a direct E_g. The CBM decreased at the M and R points for ScV, while the VBM shows a slight increase at the X, M, and R points for ScV, and ScNb. The BS of ZrNb, ZrV, HfV, HfNb, and VNb exhibited electron–pockets. The BS of Sc*M*n, Zr*M*n, and H*f*Mn showed an increase in large electron–pockets, as can be observed from the Γ–X–M–Γ point. The electron–pocket has the effect of reducing the S value, which can clearly be seen in Figure 24 and can be expressed as (Sootsman, Chung & Kanatzidis, 2009):

$$S \propto \frac{1}{\mathrm{DOS}(\mathrm{E_F})} \frac{\partial[\mathrm{DOS}(\mathrm{E_F})]}{\partial \mathrm{E_F}}, \tag{81}$$

where $\mathrm{DOS}(\mathrm{E_F})$ is the density of state at E_F. Referring to Figure 26, we can see that the electron–pocket has the effect of increasing $\mathrm{DOS}(\mathrm{E_F})$; therefore it also decreased S which can be seen by expanding this relation of $\mathrm{DOS}(\mathrm{E_F})$ and S with equation (74). In order to expand the TDOS, we calculated the partial DOS (PDOS) with electron s, p, d, and f states, as shown in Figure 29.

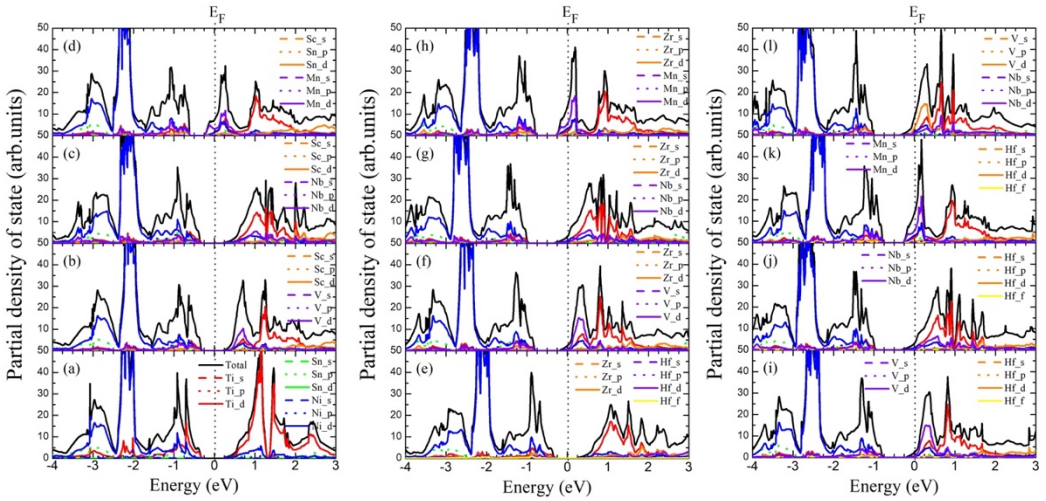

Figure 29 The partial density of state (PDOS) of TiNiSn (a) and $Ti_{0.5}TMI_{0.25}TMII_{0.25}NiSn$ composed of ScV (b), ScNb (c), ScMn (d), ZrHf (e), ZrV (f), ZrNb (g), ZrMn (h), HfV (i), HfNb (j), HfMn (k), and VNb (l).

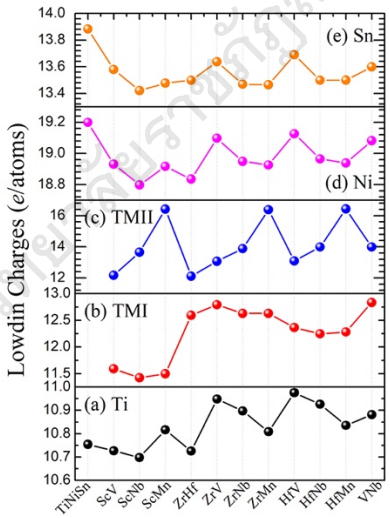

Figure 30 The calculated Löwdin charges of TiNiSn and $Ti_{0.5}TMI_{0.25}TMII_{0.25}NiSn$.

The PDOS of TiNiSn showed that Ti–d and Ni–d have high values at VBM and CBM. In addition, the Ni–d shows a high concentration at the valence band while Ti–d shows a high concentration at the conduction band. The Ti–d state decreased with co–doping. The PDOS showed that the TM occurred in the conduction band near

the CBM. The E_F was shifted up into the CBM by the TM–d state, as shown in Figures 29(d) and 30(f – l), and confirmed by Löwdin charge analysis, as shown in Figure 30. We found that the Löwdin charge of Ti increased from 10.75 to 11.0 *e*/atoms. TMII has a higher value than TMI and Ti, which affected the high PDOS around the CBM. In addition, Mn shows the highest Löwdin charge of more than 16.0 *e*/atoms and has the effect of shifting the TDOS up into E_F.

Referring to Figure 27, we can see that TiNiSn, ScV, ScNb, and ZrHf exhibit semiconductor behavior with a large S at around E_F. ScMn, ZrNb, ZrV, ZrMn, HfV, HfNb, HfMn, and VNb exhibit metal–like behavior because they have narrow S values from –200 to –20 μV K^{-1}. As is well known, the calculated σ from BoltzTraP includes the scattering time as σ/τ. Ong *et al.* (2011) evaluated τ by using the experimental data of σ ($\sigma_{\mathbf{exp}}$) via the relationship $\tau = \sigma_{\mathbf{exp}}/(\sigma/\tau)$. We used the $\sigma_{\mathbf{exp}}$ of Katayama *et al.* (2003) to evaluate the τ of TiNiSn and $Ti_{0.5}TMI_{0.25}TMII_{0.25}NiSn$, as shown in Table II. The calculated TE properties include PF, $\kappa_{\mathbf{total}}$, and ZT, as shown in Figure 31.

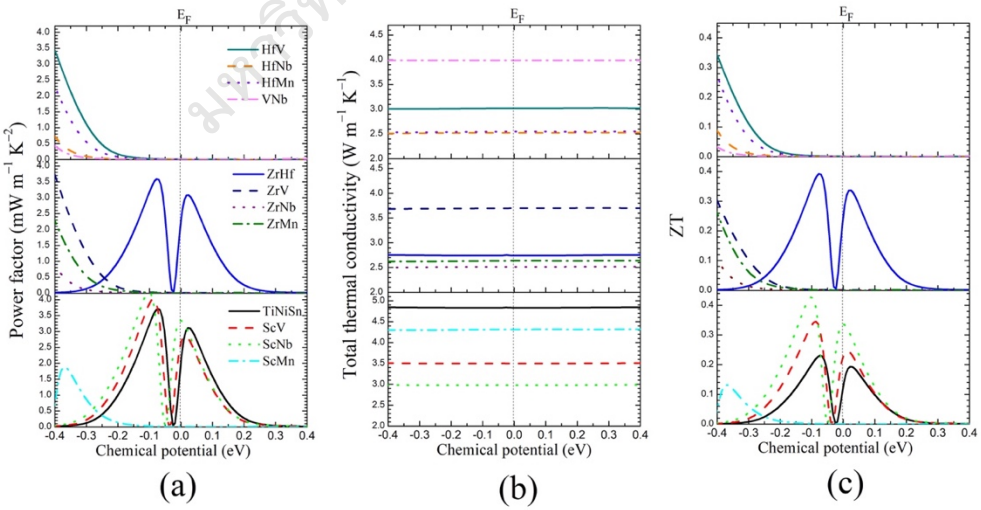

Figure 31 The power factor (a), total thermal conductivity (b), and ZT (c) versus chemical potential for TiNiSn and $Ti_{0.5}TMI_{0.25}TMII_{0.25}NiSn$, at room temperature.

The TE properties are presented versus the chemical potential between –0.4 and 0.4 eV. In Figure 31(a), the calculated PF shows high values in the chemical potential range of –0.1 to 0.1 eV for TiNiSn, ScV, ScNb, and ZrHf. Meanwhile, ScMn, ZrV, ZrNb, ZrMn, HfV, HfNb, HfMn, and VNb showed that they have a very low PF at around E_F and a high PF below –0.3 eV. The low PF is cursed with the lowest S around E_F, as shown in Figure 27. In order to evaluate the ZT, we calculated $\kappa_{\mathbf{lat}}$ using MD–GK. The calculated $\kappa_{\mathbf{lat}}$ versus time–correlation of TiNiSn and $Ti_{0.5}TMI_{0.25}TMII_{0.25}NiSn$ are shown in Figure 32. It was observed that the $\kappa_{\mathbf{lat}}$ values of ScNb, ZrHf, ZrNb, ZrMn, HfV, HfNb, HfMn are less than 3 W m^{-1} K^{-1} and quickly show a constant value. The auto–correlation function can be expressed by the equation:

$$\mathrm{J}(t) = \frac{1}{\Omega}\left[\sum_j E_j(t)v_j(t) + \sum_{j,i\neq j} r_{ij}(t)\zeta_{ij}(t)v_{ij}(t)\right], \qquad (85)$$

where $E(t)$, $v(t)$, $r(t)$, and $\zeta(t)$ are the total energy, velocity, inter–atomic distance, and inter–particle force, depending on the time–correlation for atoms i and j. The value of $\kappa_{\mathbf{tot}}$ was obtained by summing $\kappa_{\mathbf{lat}}$ and $\kappa_{\mathbf{e}}$ from equations (76) and (78), as shown in Figure 31(b). When compared with the literature, our value of $\kappa_{\mathbf{lat}}$ for TiNiSn calculated by MD–GK is less than that in the literature, as shown in Table II.

The calculated $\kappa_{\mathbf{tot}}$ is slightly higher than $\kappa_{\mathbf{lat}}$ due to the $\kappa_{\mathbf{e}}$ having a small value at room temperature. Our calculation shows that TM–co–doped TiNiSn can reduce $\kappa_{\mathbf{lat}}$ by 12.4 – 98.3% at room temperature. The optimized ZT shows a high value at around E_F, as shown in Figure 31(c) and Table 8. Our calculated PF and ZT at E_F for TiNiSn agree with the experimental data of Katayama et al. (2003) Our calculated TE properties showed that ZrHf can retain PF and reduce $\kappa_{\mathbf{tot}}$ which it affected to obtain a high ZT in good agreement with the experimental data of Sakurada and Shutoh (2005). In addition, we estimated that the ScV and ScNb co–doped Ti–site of TiNiSn as $Ti_{0.5}Sc_{0.25}V_{0.25}NiSn$ and $Ti_{0.5}Sc_{0.25}Nb_{0.25}NiSn$ should optimize ZT.

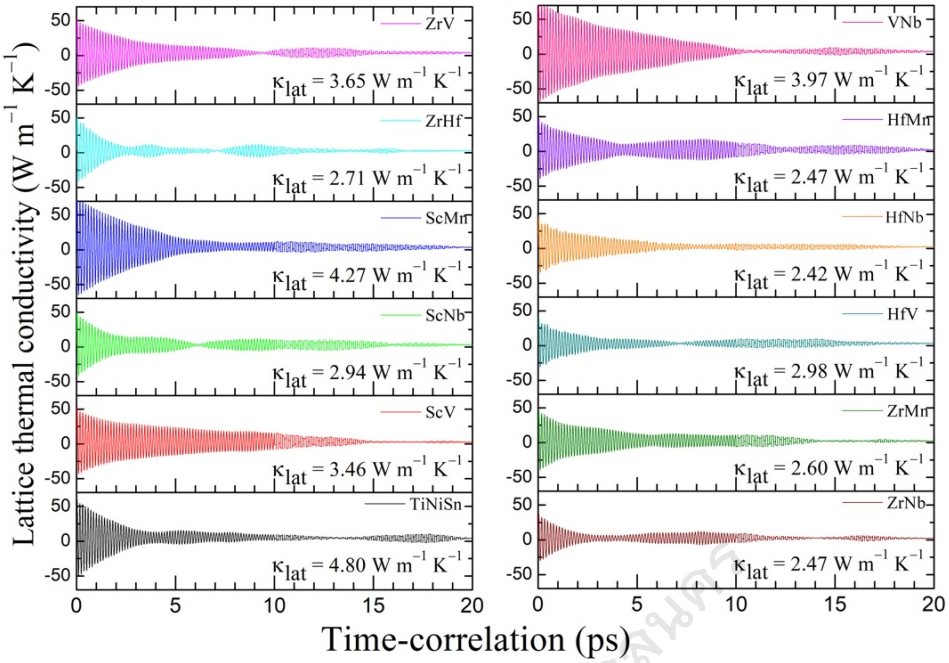

Figure 32 The lattice thermal conductivity versus time–correlation for TiNiSn and $Ti_{0.5}TMI_{0.25}TMII_{0.25}NiSn$, at room temperature.

Table 8 The scattering time, $\boldsymbol{\kappa_{lat}}$, and ZT for TiNiSn and $Ti_{0.5}TMI_{0.25}TMII_{0.25}NiSn$ (TMI and TMII are Sc, Zr, Hf, V, Nb, or Mn) at room temperature.

$Ti_{0.5}TMI_{0.25}TMII_{0.25}NiSn$	$\boldsymbol{\tau}$ (s)	$\boldsymbol{\kappa_{lat}}$ (W m^{-1} K^{-1})	ZT at E_F
TiNiSn	9.22×10^{-15}	4.8 (this work, MD–GK), 6.0 (Katayama *et al.*), 7.0 (Toher *et al.*), 6.0 (Eliassen *et al.*)	0.12
$Ti_{0.5}Sc_{0.25}V_{0.25}NiSn$	3.73×10^{-14}	3.46 (this work, MD–GK)	0.23
$Ti_{0.5}Sc_{0.25}Nb_{0.25}NiSn$	3.12×10^{-14}	2.94 (this work, MD–GK)	0.33
$Ti_{0.5}Sc_{0.25}Mn_{0.25}NiSn$	1.05×10^{-16}	4.27 (this work, MD–GK)	6.42×10^{-4}
$Ti_{0.5}Zr_{0.25}Hf_{0.25}NiSn$	1.34×10^{-14}	2.71 (this work, MD–GK), 3.0 (Schrade *et al.*)	0.23
$Ti_{0.5}Zr_{0.25}V_{0.25}NiSn$	1.77×10^{-16}	3.65 (this work, MD–GK)	4.56×10^{-5}
$Ti_{0.5}Zr_{0.25}Nb_{0.25}NiSn$	9.04×10^{-17}	2.47 (this work, MD–GK)	5.11×10^{-5}
$Ti_{0.5}Zr_{0.25}Mn_{0.25}NiSn$	8.14×10^{-17}	2.60 (this work, MD–GK)	2.91×10^{-4}
$Ti_{0.5}Hf_{0.25}V_{0.25}NiSn$	1.76×10^{-16}	2.98 (this work, MD–GK)	1.09×10^{-3}
$Ti_{0.5}Hf_{0.25}Nb_{0.25}NiSn$	9.07×10^{-17}	2.42 (this work, MD–GK)	6.41×10^{-4}
$Ti_{0.5}Hf_{0.25}Mn_{0.25}NiSn$	8.19×10^{-17}	2.47 (this work, MD–GK)	2.24×10^{-4}
$Ti_{0.5}V_{0.25}Nb_{0.25}NiSn$	8.68×10^{-17}	3.97 (this work, MD–GK)	3.54×10^{-4}

Summary

The electronic structure and thermoelectric properties of the transition metal co–doped Ti–site of TiNiSn were investigated by density functional theory, the Boltzmann transport equation, and molecular dynamics with the Green–Kubo relation. Our calculated electronic structure showed that the transition metals affect the equilibrium structural parameter, density of state, Fermi energy, and charge population. The E_g of TiNiSn is slightly reduced by ScV, ScNb, and ZrHf, that affected the high PF. The ZrNb, ZrV, HfV, HfNb, VNb, Sc*M*n, Zr*M*n, and Hf*M*n created electron–pockets around E_F and also reduced S, which caused the reduction in PF. The calculated κ decreased with co–doping by transition metals. The optimized ZT showed that the TiNiSn and ZrHf have high values around E_F. We proved that $Ti_{0.5}Sc_{0.25}V_{0.25}NiSn$ and $Ti_{0.5}Sc_{0.25}Nb_{0.25}NiSn$ show good potential as *n*–type TE materials.